

Cubic boron nitride: a new prospective material for ultracold neutron application

Yu. Sobolev^{1,a,*}, Th. Lauer², Yu. Borisov³, M. Daum⁴, N. du Fresne¹, L. Göttl^{2,8}, G. Hampel², W. Heil¹, A. Knecht^{4,5}, M. Keunecke⁶, J. V. Kratz², T. Lang¹, M. Meister¹, Ch. Plonka-Spehr², Yu. Pokotilovski⁷, P. Reichert², U. Schmidt⁸, Th. Krist⁹, N. Wiehl², J. Zenner¹

¹Institute for Physics, Johannes Gutenberg-Universität Mainz, Staudingerweg 7, D-55128 Mainz, Germany

²Institute for Nuclear Chemistry, Johannes Gutenberg-Universität Mainz, Fritz-Strassmann-Weg 2, D-55128 Mainz, Germany

³Petersburg Nuclear Physics Institute, 188300 Gatchina, Leningrad region, Russia

⁴PSI, Paul Scherrer Institut, CH 5232 Villigen, Switzerland

⁵University of Zurich, Switzerland

⁶Fraunhofer-Institut für Schicht- und Oberflächentechnik, Bienroderweg 54e, D-38108 Braunschweig, Germany

⁷JINR, Joint Institute for Nuclear Research, 141980 Dubna, Moscow region, Russia

⁸Physical Institute, Universität Heidelberg, Philosophenweg 12, D-69120 Heidelberg, Germany

⁹Hahn-Meitner-Institut Berlin, Glienicker Str. 100, D-14109 Berlin, Germany

Abstract

For the first time, the neutron optical wall-potential of natural cubic boron nitride (cBN) was measured at the ultracold neutron (UCN) source of the research reactor TRIGA Mainz using the time-of-flight method (TOF). The samples investigated had a wall-potential of (305 ± 15) neV. This value is in good agreement with the result extracted from neutron reflectometry data and theoretical expectations. Because of its high critical velocity for UCN and its good dielectric characteristics, cubic boron nitride coatings (isotopically enriched) will be useful for a number of applications in

UCN experiments.

*Corresponding author; email: iouri@uni-mainz.de

^aOn leave from Petersburg Nuclear Physics Institute, Gatchina, Russia

PACS numbers and key words:

28.20.Gd, Neutron transport: diffusion and moderation

14.20.Dh, Protons and neutrons

29.25.Dz, Neutron sources

1. Introduction

Ultracold neutrons can be stored in material bottles for times approaching the beta decay lifetime of the neutron. The storage is based on the reflection of the UCN by selected materials under any angle of incidence. The reflection is caused by the coherent strong interaction of the neutron with the atomic nuclei. Quantum mechanically, this can be described by an effective potential which is commonly referred to as Fermi pseudo potential or the material optical potential, U_f .

The storage of neutrons with very low energies was predicted by Zeldovich [1] in 1959 and experimentally realized simultaneously by groups in Dubna [2] and in Munich [3] in 1968. Since then, UCN have become a unique tool for fundamental neutron physics, e.g., experiments looking for a permanent electric dipole moment of the neutron (nEDM) [4] or measuring the neutron lifetime [5,6]. UCN have velocities typically below 7 m/s, corresponding to energies below 250 neV.

The material optical potential U_f can be expressed as $U_f = V - iW$ [7], where the wall-potential V describes the reflecting and W the absorbing behaviour of the material and is given by

$$V = \frac{2\pi\hbar^2}{m} \cdot \sum_i N_i b_i, \quad W = \frac{\hbar}{2} \cdot \sum_i N_i \sigma_i v_{\text{th}}. \quad (1)$$

Here, m is the neutron mass, N is the scattering center density, b is the bound coherent scattering length, σ is the sum of the absorption, σ_a , and the inelastic scattering cross section, σ_{ins} , at thermal neutron velocities, v_{th} . The sum over i includes all specific nuclei of the chemical composition. Neutrons with a normal velocity component below a critical value $v_c = (2V/m)^{1/2}$ are totally reflected from the surface. The loss probability per reflection is expressed by the energy-independent loss coefficient $\eta = W/V$.

The v^2 dependence of the UCN velocity spectrum leads to a storable UCN density which scales with $V^{3/2}$. Therefore, V has to be as high as possible to increase statistics in UCN experiments. At the same time, the η value has to be low enough to reduce absorption and upscattering losses. Besides this, specific experiments like the nEDM require additional properties of the materials, e.g., high electrical

resistivity (also against surface currents), non-magnetic properties, and high vacuum compatibility.

The material with the so far highest known wall-potential commonly used in UCN experiments, is ^{58}Ni with $V = 346$ neV corresponding to a critical velocity of $v_c = 8.1$ m/s. Nickel, however, is magnetic and conductive. So far, only beryllium oxide (BeO , $V = 261$ neV, $\eta < 1 \times 10^{-4}$) satisfies all criteria mentioned above. But its toxicity may be prohibitive.

Looking for other non-toxic, non-magnetic materials with high wall potentials and high electrical resistivity, we got interested in cubic boron nitride (cBN). Due to its hardness and high wear resistance, cBN is under development as a super-hard coating (micro-hardness > 50 GPa, [8]) for cutting tools in the metal machining industry.

Natural boron consists of two isotopes of abundance ratio: $^{10}\text{B}/^{11}\text{B} = 0.248$. The calculation of the pseudo-potential of this chemical composite using Eq. (1) and the given material parameters, $\rho \approx 3.5$ g/cm³ [9, 10], $N \approx 8.5 \times 10^{22}$ cm⁻³, $b(^{10}\text{B}) = -0.1$ fm, $b(^{11}\text{B}) = 6.65$ fm, $b(\text{N}) = 9.36$ fm, yields $V = 324$ neV and $\eta \approx 1.5 \times 10^{-2}$. The value for η reflects the enormously high absorption cross section of ^{10}B , $\sigma_a = 3840$ barn [11].

This drawback can, in principle, be overcome by using isotopically enriched ^{11}B in the composite ($\sigma_a = 0.0055$ barn), which results in an even higher wall-potential of $V = 351$ neV. The value of $\eta \approx 3.3 \times 10^{-5}$ in this case is mainly dominated by the absorption of ^{14}N ($\sigma_a = 1.9$ barn) for an ^{11}B enrichment of > 99.95 %. As a first step, we started with the investigations of natural cBN.

2. Experiments

We carried out two experiments to measure the critical velocity of UCN reflected from natural cBN using (i) a time-of-flight (TOF) measurement in order to determine the transmission of ultracold and very cold neutrons (VCN) through a silicon wafer (380 μm) coated with natural cBN of thickness 300 nm and (ii) cold neutron

reflectometry with the same sample. For comparison, a natural nickel coated sample with a layer thickness of 500 nm was investigated using the TOF method.

The cBN films were prepared in a reactive r.f. diode sputtering system using an electrically conducting boron carbide (B_4C) target. In order to reach good adhering cBN layers, a special process was used starting with an interlayer of boron carbide and continuing with graded BCN interlayers, where the carbon is replaced by nitrogen by means of an incremental change from argon to nitrogen as sputter gas. Further information on the process and the sputtering facility can be found in Refs. [8, 12, 13]. With this method, cBN layers of up to 2 μm thickness and a cubic phase content of approximately 90 % (measured by IR spectroscopy [8, 12, 13]), corresponding to a density of 3.3 g/cm^3 , are produced.

The Nickel coating was produced at Hahn-Meitner-Institut (HMI) by conventional DC magnetron sputtering. With this technique it is possible to reach coating densities close to 100% of bulk material.

2.1 The time-of-flight experiment

In the time-of-flight (TOF) experiment, we determined the neutron optical potential via the critical neutron velocity from the transmission of slow neutrons through the sample. The experiment was performed at the solid deuterium UCN source at beamport C [14] of the research reactor TRIGA Mainz [15, 16]. This reactor can be operated at a steady-state power of 100 kW or in pulsed mode with a maximum power of 250 MW and an energy release of 10 MWs [17].

In principle, a TOF measurement can be performed both in the pulsed or in steady state mode of the reactor. In the pulsed mode, the minimal overall length of the flight path is from the layout of the reactor (biological shield, cryostat, etc., cf. [14]) more than 6 m. In such a long UCN guide, part of the neutrons are repeatedly diffusely scattered back and forth and the neutron guide acts also as a neutron storage chamber. This leads to a delay of these scattered neutrons in reaching the detector apparently at a lower velocity which influences the results.

In the steady state mode using a chopper for the TOF information, the TOF path length can be chosen to be much shorter and the delay effect is negligible.

Therefore in this experiment, the reactor was operated in the steady-state mode of 100 kW thermal power. In all measurements, the same amount of solid deuterium (4 mol) in the UCN source was used. Outside the biological shield of the reactor core, at a distance of ~ 4 m from the solid $^2\text{H}_2$ converter, the in-pile part of the neutron guide is terminated by an aluminium window at room temperature. We used a time-of-flight spectrometer with a chopper [18] similar to that used in Refs. [19–21]. The neutrons were guided via electro-polished stainless steel tubes with inner diameter 66 mm from the UCN source to the TOF spectrometer. The arrangement is schematically sketched in Fig. 1. Neutrons enter from the left and pass the TOF spectrometer towards a Cascade-U detector [22] at the end of the flight path. The flight path between chopper and detector was (1006 ± 3) mm. The Al entrance window of the detector was 0.1 mm thick with an energy barrier of 54 neV from the material optical potential of aluminium and caused some reduction of the detector efficiency. With this setup, the (averaged) velocity component along the forward direction can be measured.

The coated silicon wafers (diameter 76 mm) were inserted in a foil holder placed in front of the chopper operating at a duty cycle of 4.0 % and at a frequency of 1.0 Hz. For the correct determination of a velocity distribution with the TOF method, we assume a high guide transmission for UCN, *i.e.* a high percentage of specular reflections in the UCN guide system, which is experimentally supported by Ref. [23]. Without sample, the count rate in our TOF spectrometer was about 45 s^{-1} .

As DAQ system, we used a standard TOF card from the FAST company. The TOF spectrum was started with the pulse from the chopper indicating the chopper status 'open'. Neutrons were registered with a dwell time of 1.5 ms according to their arrival time in the detector. Figure 2 shows the time-of-flight spectra without and with samples, *i.e.*, the nickel and cubic natural-boron nitride sample.

2.1.1 Background subtraction

The data in Fig. 2 show backgrounds originating mainly from three effects: (i) a constant background which originates from thermal neutrons which are present inside the experimental area during reactor operation and cannot be suppressed completely; (ii) an almost constant background from neutrons which were diffusely scattered, *i.e.*, the neutron guide acts also as a UCN storage chamber which is repeatedly filled by the chopper cycles and emptied through the opening to the detector; (iii) the periodic humps in the spectra stem from very cold neutrons which could penetrate thinner parts of the rotating chopper plates. These were to compensate for the openings in the plates in order to avoid unbalances (they are now painted with the high absorption material Gd_2O_3).

We divided the time scale of the three spectra into 10 regions and fitted the background to constant values in seven regions left and right of the TOF peaks. The background underneath the peaks was subtracted by interpolation. The reduced χ^2 of the fits ranged from 1.04 to 3.1 with one as high as 5.7. The χ^2 values, partly significantly larger than 1, originate mainly from sparks in the detector during the first days of operation. These sparks were produced by short high voltage breakthroughs from the gas electron multiplier (GEM) to the read-out structure of the detector and led to an increased number of events in several channels, see, e.g., at $t = 0.12$ s in the cBN data in Fig. 2. Surface contaminations (dust particles) on the GEM foil lead to a locally increased electric field and sparks which also clean the surface. Consequently, these contaminations were reduced and the detector was more stable after several days. In order to take these non-statistical uncertainties into account, we firstly replaced the very few data which differed by more than 5 standard deviations from their neighbours by the average of the neighbouring data. Secondly, we increased the uncertainties of the respective data points by a factor $\sqrt{\chi^2}$, as recommended, *e.g.*, by Refs. [24,25]. The data after background subtraction used for the further analysis are shown in Fig. 3.

2.1.2 Time calibration

Time calibration of the system, see Ref. [19], was obtained by comparing (i) at one distance the spectra taken at two different chopper frequencies; (ii) at one chopper frequency the TOF spectra taken at the two distances. We obtained eight partially dependent calibration measurements by comparing the TOF spectra at different chopper frequencies, three pairs at each distance: (a) 1.00 Hz, 0.75 Hz, (b) 1.00 Hz, 0.50 Hz, and (c) 0.75 Hz, 0.50 Hz, and additional three calibration measurements (one per frequency) by comparing the TOF spectra at the two distances.

Since the electronic signal from the chopper is produced by a photoelectric barrier triggered by an interrupter on one of the rotating chopper discs, we obtain a time difference, δt , between the electronic trigger signal from the chopper and its real opening time. The value of δt depends on the chopper frequency. Averaging all available and independent information we find $\delta t(1\text{Hz}) = (0.191 \pm 0.003)$ s. Recently, the calibration measurements were repeated at ILL with frequencies 0.5 Hz, 1 Hz, and 1.25 Hz confirming the earlier result [19].

2.2 Analysis of the time-of-flight experiment

In order to extract the values of the optical potential from the layers of interest, we developed an analysis procedure following three steps. In the first step, we approximated the measured data with no sample and after background subtraction with a cubic spline function based on nine data points in order to obtain an analytic expression for the data. The χ^2 per degree-of-freedom was 2.8 which on the one hand originates from sparks in the detector and on the other hand reflects the rather simplified parameterization of the spectrum by the spline which, however, is sufficient for our purposes. In order to take this non-statistical uncertainty into account, we increased the uncertainties of the data points by a factor $\sqrt{\chi^2}$, see above.

In a second step, we calculate the transmission of the UCNs through layers. For given values of the Fermi potential of each layer, we developed procedures to perform a one-dimensional numerical solution of the Schrödinger equation. Hereby,

we include surface roughness via smearing of the potential step at the border of adjacent layers. Matching the numerical solution of the Schrödinger equation outside the layers with the well known analytical solution for plane wave propagation allows us to calculate the value for the transmission.

In the third step, we compare our model with the measured data. For this purpose, we convolute the product of the transmission function (step 2) and the initial spectrum (step 1) with the opening function of the chopper, see Fig. 4. The free parameters of the fit were the mean free paths in the coated layers (cBN, Ni), the loss parameter η and the roughness of the sample. The values of these parameters were obtained by comparison of our model with the data and minimisation using standard least square fitting techniques. The experimental data with the final fit are shown in Fig. 5. In Fig. 6, the curves for the velocity dependent transmission for the different measured samples as derived from the analysis are shown.

Due to its ferromagnetic properties, the neutron transmission through the Ni sample results in the sum of the transmission for the different neutron spin states (with their different optical potential values). From the measured data, we extract the value of the optical potential for spin down of (207 ± 2) neV and for spin up (284 ± 2) neV (here ± 2 neV includes uncertainty of fit only). The reduced χ^2 of the fit is 4.5, see above. This results correspond to a Ni bulk density of 98 % of the nickel density.

For our cBN sample, we obtain a value for the optical potential of (305 ± 2) neV. From this, we calculate a value of 90 % for the bulk density. The reduced χ^2 of the fit was 1.7.

In order to take these χ^2 values as non-statistical uncertainties into account, we increase the uncertainties (± 2 neV) by the factors $\sqrt{\chi^2}$. The main contributions to the total uncertainty arise, however, from the time calibration of the TOF spectrometer, $\delta V = 15$ neV; the uncertainty originating from the flight path uncertainty is 2 neV. Thus, the total uncertainties of our values for the optical potentials are $\Delta V \approx 15$ neV. The final results of our analysis are summarized in Table I. While

the optical potential of cBN has never been measured before, the values for Ni are in excellent agreement with literature values [20].

2.3 The neutron reflectometry experiment

The second experiment using neutron reflectometry was performed at the neutron reflectometer V14 at the cold beam at the HMI. This method measures the critical angle for total reflection of cold neutrons at grazing incidence, where the velocity component normal to the surface is comparable to the velocity of UCN. Unlike UCN, cold neutrons do not suffer from small angle scattering inside the sample. Due to this fact, cold neutron reflectometry can be seen as cross-checke to the transmission measurements.

The neutron critical angle of total reflection, θ_c , is directly connected with the scattering length density, *i.e.*, the term $N \cdot b$ in equation (1), via the formula

$$\frac{\sin \theta_c}{\lambda} = \sqrt{\frac{N \cdot b}{\pi}} \quad (2)$$

where λ is the neutron wavelength (4.9 Å at V14). By measuring θ_c for the samples under investigation, V can be determined using Eq.1:

$$V = \frac{2\pi^2 \hbar^2 \sin^2 \theta_c}{m \cdot \lambda^2} \quad (3)$$

The reflectivity function for the analysis of the data was derived with the same quantum mechanical calculation as mentioned above. However, because of the divergent beam profile, the obtained reflectivity function has to be convoluted with the known neutron beam profile.

In the fit, the free parameters were (i) the scattering length density $N \cdot b$, cf. Eq. 2, and (ii) the roughness and composition of the surfaces (substrate and coating). The model of the cBN sample is represented by three layers, air, cBN, and silicon. The scattering lengths, b , for air, boron, nitrogen, and silicon were taken from the literature [28]. The reduced χ^2 of the fit to the reflectivity data is 3.0. The uncertainties of cold neutron reflectometry depend strongly on the flatness of the samples under investigation. Silicon wafers usually have very smooth surfaces but not necessarily a high flatness over the whole coated sample. This increases the

uncertainty of the result. In order to take such an (unknown) comparative uncertainty into account, the experimental uncertainties were scaled [24, 25] to obtain a χ^2 of one. Figure 7 shows the experimental data and the fit. The extracted value of V for the reflectometer data is shown in Table 1.

3. Conclusions and outlook

The optical potential value V of natural cubic boron nitride was determined experimentally for the first time via the energy dependent transmission of very slow neutrons through a cBN layer, $V_{\text{trans}} = (305 \pm 15)$ neV and by cold neutron reflectometry, $V_{\text{refl}} = (300 \pm 30)$ neV. Both values agree with each other and are in excellent agreement with theoretical expectations, $V = 308$ neV, obtained from Eq. 1 and for the fraction of the cubic phase, which was determined independently by infrared spectroscopy to be about 90 % [8–10]. Using isotopically enriched $c^{11}\text{BN}$ samples with a fraction of $^{11}\text{B} > 99.95$ %, we expect a 10 % increase of V and a significantly reduced loss value η , as shown in Fig. 6. This will be demonstrated in the near future.

In addition to the experimental determinations of the optical potential, the insulator properties of the cBN samples were investigated using a high resistance meter 4339 A in combination with the resistivity cell 16008B (Hewlett Packard). We found values for the specific resistivity $R > 3.4 \cdot 10^{16}$ ohm-cm. This is comparable to other high resistivity values, *e.g.* of natural diamond or quartz.

In conclusion, cubic boron nitride is a very promising material for coatings with high optical potential and high resistivity.

Furthermore, it is certainly worth while to investigate cubic carbon nitride, $c\text{C}_3\text{N}_4$, and isotopically pure $^{11}\text{B}_4\text{C}$ as further coating materials for the physics with ultra-cold neutrons. From ref. [27] we expect, that one can obtain an optical potential value of $c\text{C}_3\text{N}_4$ as high as $V \approx 391$ neV ($b(\text{C}) = 6.646$ fm, $\rho(c\text{C}_3\text{N}_4 \approx 4$ g/cm³ [28]) with η being similar to the isotopically pure cubic boron nitride. For a coating with boron carbide, $^{11}\text{B}_4\text{C}$, an very low loss parameter η is expected,

$\eta \approx 10^{-7}$ ($\sigma_a = 0.0035$ barn) with the optical potential $V \approx 235$ neV ($\rho = 2.52$ g/cm³).

Acknowledgements

We thank the crew of the reactor TRIGA Mainz, J. Breuel, H. O. Kling, A. Schmidt, and H.-M. Schmidt for their help during the experiments. The experiment benefitted from the help of M. Meier, PSI, in building the chopper. This work would not have been possible without help from E. Gries, who supplied the liquid helium for our superthermal UCN source. This work was supported by the DFG under the contract numbers KR 1458/8-2 and HE 2308/2-3.

References

- [1] Ya. B. Zeldovich, Sov. Phys. JETP **9**, 1389 (1959).
- [2] V. I. Lushikov *et al.*, JETP Lett. **9**, 23 (1969).
- [3] A. Steyerl, Phys. Lett. B **29**, 33 (1969).
- [4] C. A. Baker *et al.*, Phys. Rev. Lett. **97**, 131801 (2006).
- [5] S. Arzumanov *et al.*, Phys. Lett. B **483**, 15 (2000).
- [6] A. Serebrov *et al.*, Phys. Lett. B **605**, 72 (2005).
- [7] E. Fermi, Ricerca Scientifica **7**, 13 (1936).
- [8] M. Keunecke *et al.*, Thin Solid Films **398-399**, 142 (2001).
- [9] X. Jiang *et al.*, J. of Appl. Phys. **93**, 1515 (2003).
- [10] G. Lehmann *et al.*, Appl. Phys. A: Materials Science & Processing, **74**, 41 (2002).
- [11] <http://www.ncnr.nist.gov/resources/n-lengths/>
- [12] K. Yamamoto *et al.*, Surface and Coatings Technology **142-144**, 881 (2001).
- [13] K. Yamamoto *et al.*, Thin Solid Films **377-378**, 331 (2000).
- [14] A. Frei *et al.*, Eur. Phys. J. A **34**, 119 (2007).
- [15] K. Eberhardt, A. Kronenberg, Kerntechnik **65**, 263 (2000).
- [16] G. Hampel *et al.*, Int. J. for Nucl. Power, ISSN 1431, atw 5 (2006).
- [17] H. Menke *et al.*, Kerntechnik **17**, No. 6 (1975).
- [18] P. Fierlinger *et al.*, Nucl. Instr. Meth. Phys. Res. A **557**, 572 (2005).
- [19] I. Altarev *et al.*, Eur. Phys. J. A **37**, 9 (2008).

- [20] F. Atchison *et al.*, Nucl. Instr. and Meth. in Phys. Res. B **260**, 647 (2007).
- [21] F. Atchison *et al.*, Phys. Lett. B **642**, 24 (2006).
- [22] <http://www.n-cdt.com>
- [23] I. Altarev *et al.*, Nucl. Instr. and Meth. in Phys. Res. A **578**, 450 (2007).
- [24] The Particle Data Group, Phys. Lett. B **592**, 14 (2004).
- [25] A. H. Rosenfeld, Ann. Rev. Nucl. Sci. **25**, 555 (1975).
- [26] A. Steyerl, Z. Physik **254**, 169 (1972).
- [27] Julong He *et al.* Appl. Phys. Lett. **88**, 101906 (2006).
- [28] V. Sears, Neutron News **3**, 29 (1992).

Transmission experiment				
Sample	$V(\text{Eq.}(2))[\text{neV}]$	$V(\text{exp})[\text{neV}]$	$v_c(\text{exp})[\text{m/s}]$	$\Omega[\text{Ohm}\cdot\text{cm}]$
Ni(spin up)	289	(284 ± 15)	(7.37 ± 0.19)	–
Ni(spin down)	211	(207 ± 15)	(6.29 ± 0.23)	–
cBN*)	308	(305 ± 15)	(7.64 ± 0.19)	$> 3.4 \cdot 10^{16}$
diamond	305	--	--	$3.2 \cdot 10^{16}$
Cold neutron reflectometry				
cBN*)	308	(300 ± 30)	(7.58 ± 0.38)	–

*)90% cubic phase

Table 1: Measured wall-potentials V of natural Ni, cBN, diamond and resulting critical velocities v_c together with the measured specific resistivities for cBN and diamond. In order to give more confidence on our analysing procedure, a Ni layer was measured additionally to verify V_{Ni} as expected from literature. The resulting error on V (30 neV) measured using cold neutron reflectometry mainly comes from the uncertainty to give an absolute value on the angle of grazing incidence.

Figure captions:

Fig. 1:

Sketch of the experimental setup for the time-of-flight experiment with a chopper.

Fig. 2:

Measured time-of-flight data (i) without sample (quads), (ii) with the nickel coated silicon wafer (triangles) and the cBN coated one (circles).

Fig. 3:

Measured time-of-flight data after background subtraction (i) without sample (quads), (ii) with the nickel coated silicon wafer (triangles) and the cBN coated one (circles).

Fig. 4:

Opening function of the chopper measured at a frequency of 0.1 Hz. In the analysis, the opening function is approximated by the trapezium as indicated.

Fig. 5:

Time-of-flight data of very slow neutrons through coated silicon wafers and the fit to the data. Top: 500 nm nickel coated on a 380 μm silicon wafer. Bottom: 350 nm cBN on a 380 μm silicon wafer. The corresponding TOF-data without sample used to calculate the spline fitting function for unfolding the data with the time acceptance of the chopper are shown in both plots. The measured data were corrected for the chopper time offset δt (see text).

Fig. 6:

Calculated transmission of the measured silicon wafers coated with Ni (500 nm) and cBN (300 nm) layers. The calculation was performed by using the obtained fit parameters. The theoretical transmission of an isotopically enriched $c^{11}\text{BN}$ (300nm) layer was calculated from literature cross sections. The saw-shape behaviour of transmission curves in some places is the result of quantum interference at thin layers.

Fig. 7:

Measured cold neutron reflectometry data from a silicon wafer coated with 300 nm of cBN and the corresponding fit.

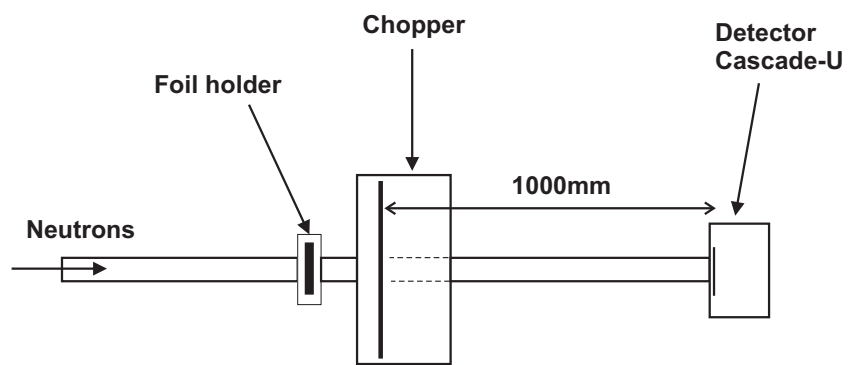


Figure 1:

Sketch of the experimental setup for the time-of-flight experiment with a chopper.

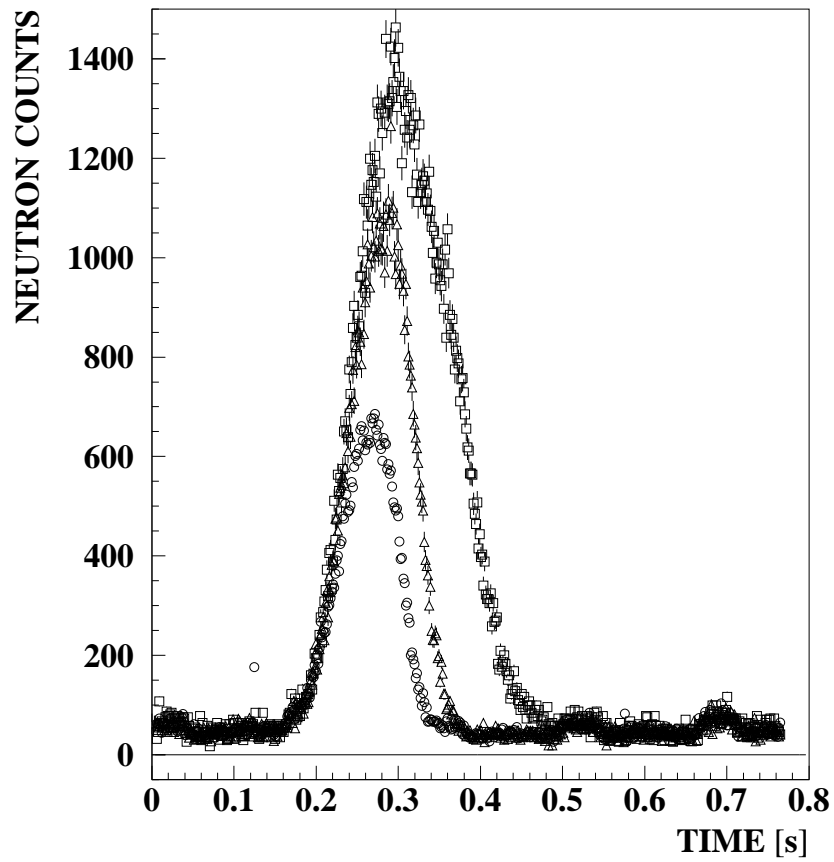


Figure 2:

Measured time-of-flight data (i) without sample (quads), (ii) with the nickel coated silicon wafer (triangles) and the cBN coated one (circles).

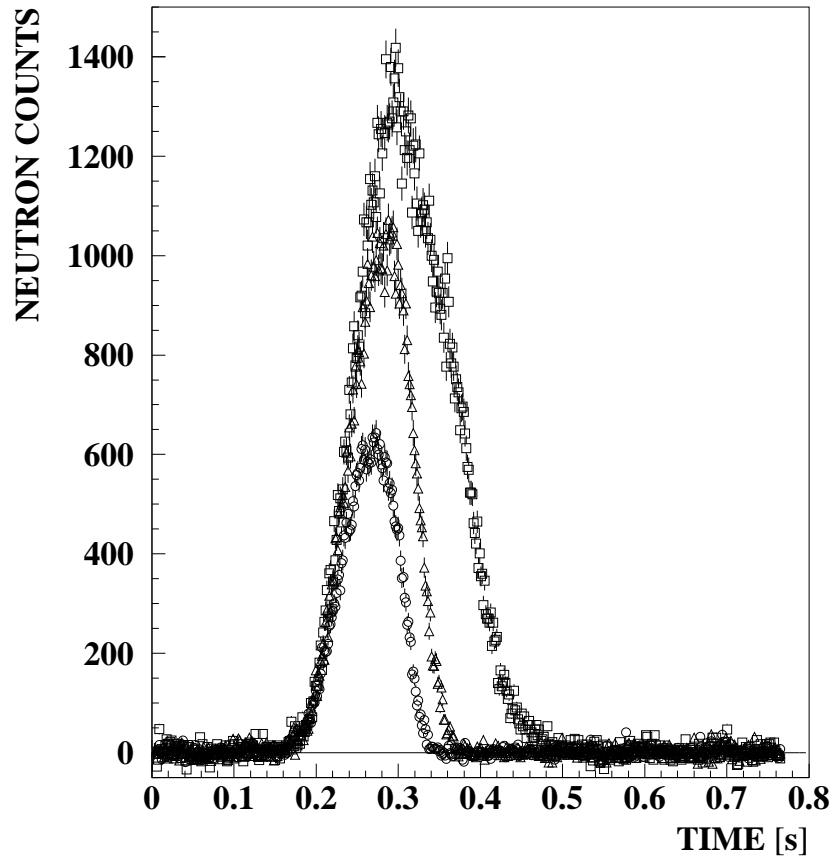


Figure 3:

Measured time-of-flight data after background subtraction (i) without sample (quads), (ii) with the nickel coated silicon wafer (triangles) and the cBN coated one (circles).

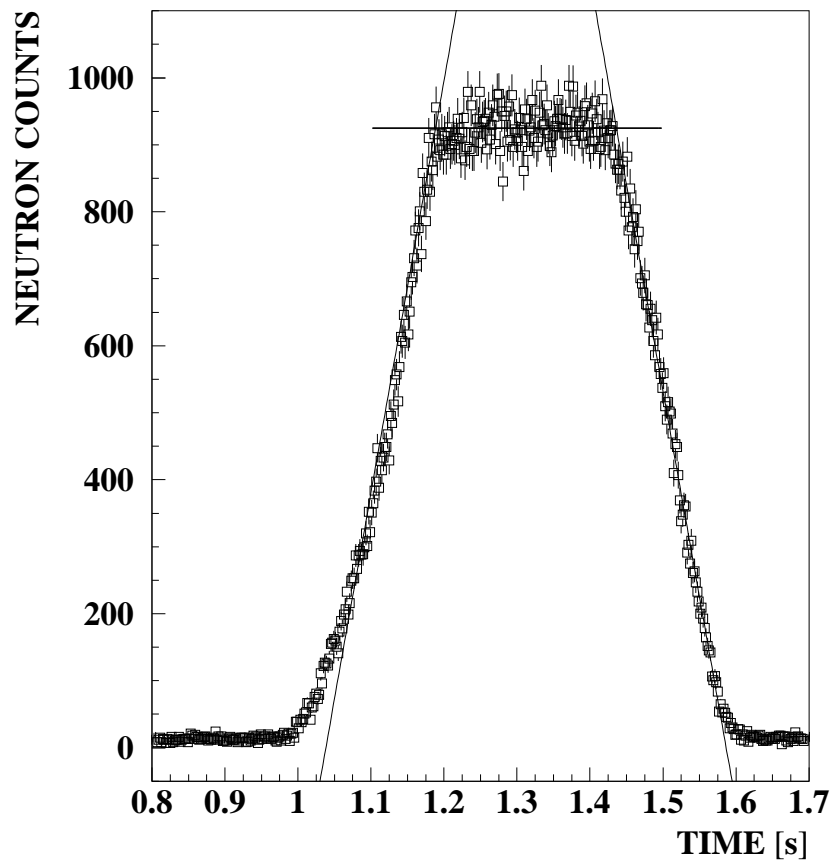


Figure 4:

Opening function of the chopper measured at a frequency of 0.1 Hz. In the analysis, the opening function is approximated by the trapezium as indicated.

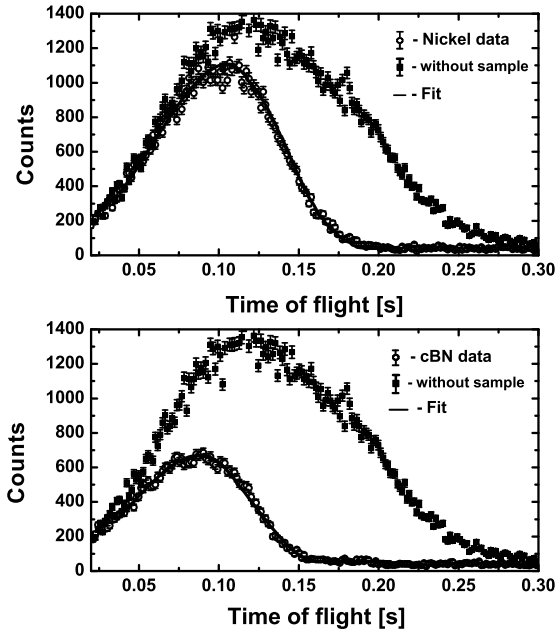


Figure 5:

Time-of-flight data of very slow neutrons through coated silicon wafers and the fit to the data. Top: 500 nm nickel coated on a 380 μm silicon wafer. Bottom: 350 nm cBN on a 380 μm silicon wafer. The corresponding TOF-data without sample used to calculate the spline fitting function for unfolding the data with the time acceptance of the chopper are shown in both plots. The measured data were corrected for the chopper time offset δt (see text).

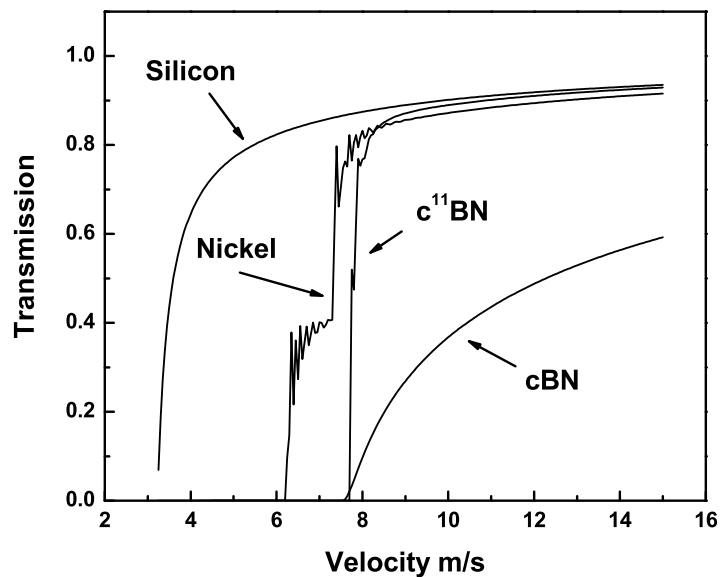


Figure 6:

Calculated transmission of the measured silicon wafers coated with Ni (500 nm) and cBN (300 nm) layers. The calculation was performed by using the obtained fit parameters. The theoretical transmission of an isotopically enriched c¹¹BN (300nm) layer was calculated from literature cross sections. The saw-shape behaviour of transmission curves in some places is the result of quantum interference at thin layers.

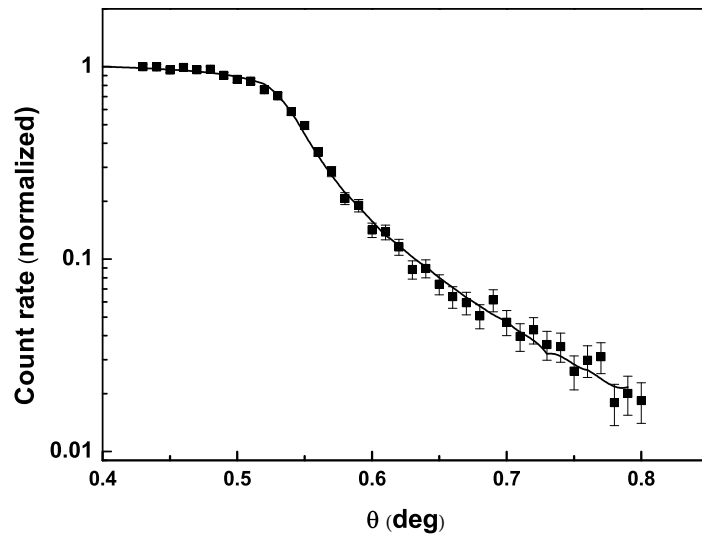


Figure 7:

Measured cold neutron reflectometry data from a silicon wafer coated with 300 nm of cBN and the corresponding fit.